2025 IEEE/SICE International Symposium on System Integration (SII)
January 21-24, 2025, Munich, Germany

Image-based Response Measurement of Liquid Lens and Iterative Calibration of Scanning Focus Tracking for Dynamic Iris Authentication

Tomohiro Sueishi[1], Keiko Yokoyama[2], Shoji Yachida[2], and Masatoshi Ishikawa[1]

***Abstract*— There is an increasing demand for iris authentication in dynamic environments, such as when people are walking. High-speed focus control using a liquid lens is one solution for such dynamic iris authentication, but it is necessary to increase the frequency of capturing in-focus iris images considering the blinking of the eye. In this paper, we propose a simple response measurement method of the liquid lens using a large and tilted checker pattern, and an iterative calibration method of sinusoidal parameters in scanning focus tracking control using the liquid lens. We have experimentally confirmed step and sinusoidal responses of the liquid lens, and demonstrated sufficient and high-frequency AR marker (alternative to iris) recognition performance of the scanning focus tracking control for manual marker movement and zooming adjustments with a motorized lens.**

I. INTRODUCTION

Micro and complex spatial textures can encompass a wealth of information that can be read by a camera. Therefore, we can use them not only to add information to objects through artificial two-dimensional codes such as augmented reality (AR) markers or quick response (QR) codes, but also as biometric authentication features such as fingerprints or irises. Such textures should be recognized not only under static conditions but also under dynamic conditions. The recognition of moving AR markers enables interactive augmented reality and user interfaces, the recognition of moving QR codes enables efficient product management, and the biometric authentication of moving people enables efficient walk-through gates [1].

Texture recognition under dynamic conditions requires adaptive control of the angle of view, focus, and zoom conditions; pan/tilt control to keep the texture within the angle of view [2], focus control to keep it within the depth of field [3], and zoom control to capture the texture with sufficient spatial resolution. Especially in focus control, liquid lenses or focus-tunable lenses that use liquid instead of solid lenses enable high-speed focus control [3], and response measurement methods and optimal control methods for predetermined input signals have also been proposed [4].

However, several challenges remain to realize remote dynamic iris authentication as a practical application of high-speed variable-focus lenses. It is difficult to use predesigned input signals [4] because of the need to provide dynamic feedback control for a moving (e.g., advancing) eye. As iris authentication requires the most in-focus image (even a single image is enough), focus scanning is desirable to eliminate the effect of spatial calibration residuals due to multi-camera triangulation [1]. In addition, focus scanning should be performed as frequently as possible to prevent the most in-focus image acquisition failure due to blinking (about 200 ms [5]). Furthermore, high-frequency focus scanning must be robust to dynamic control of zooming [6] so that the camera can capture the iris at the appropriate resolution [7], [8] at different depth positions. To achieve this, it is desirable to measure temporal changes in the optical power of the liquid lens as imaging optics (including the zoom lens).

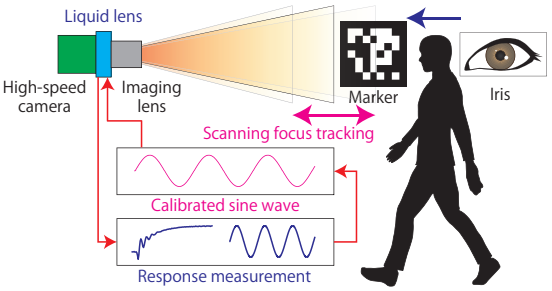

Fig. 1. A concept of the proposed method.

In this paper, we focus on the optics control in the dynamic iris authentication [1], and we propose a method to measure the responses of a liquid lens even equipped with an imaging lens, and an iterative calibration method for scanning focus tracking control of the liquid lens. The concept of the proposed method is shown in Fig. 1. The response of the liquid lens is evaluated by comparing the degree of focus at different positions using images of a large inclined checker pattern taken by a high-speed camera under static conditions. To keep the tracking target in focus, a sinusoidal wave is applied to the liquid lens to scan the focus. The reference position of the sinusoidal wave is continuously updated based on the contrast peak position estimated from the scanned images. For calibration of focus scanning parameters, we refer to a closed-loop optimization procedure [9] that searches for appropriate values of the liquid lens responses, including phase delay (i.e., temporal latency), sinusoidal reference position, sinusoidal frequency, and amplitude, under real-time visual feedback conditions.

II. RELATED WORK

A. Walk-through Iris Authentication

The iris is a doughnut-shaped region of approximately 12 mm in diameter located in the human eye. Each individ-

[1]T. Sueishi and M. Ishikawa are with Research Institute for Science and Technology, Tokyo University of Science, Niijuku 6-3-1, Katsushika-ku, Tokyo 125-8585, Japan. sueishi@ishikawa-vision.org

[2]K. Yokoyama and S. Yachida are with Visual Intelligence Research Laboratories, NEC, 1753 Shimonumabe, Nakahara-ku, Kawasaki-shi, Kanagawa, 211-8666, Japan. k.yokoyama@nec.com

ual, even identical twins, have different patterns, and these patterns do not change throughout life, making it a suitable region for highly accurate biometric authentication. For iris authentication, the iris must be imaged in focus and at high resolution. [8] specifies that the iris radius should be imaged at 80 pixels or more.

Conventional iris authentication methods are to have the person to be authenticated stand still within the in-focus range near the camera and capture an iris image. However, for use in environments where many people pass through (e.g., entry and exit at airports), positioning takes too much time. Therefore, in recent years, the demand for IRIS At A Distance (IAAD) [10] has increased, which provides authentication from a distance for moving people. Especially when assuming a walk-through gate, it is difficult for a general imaging system with an autofocus function to stably track a walking person. Therefore, the mainstream method is to extract the in-focus image from an image sequence taken in high-speed succession at a fixed focus, but challenges to diverse statures and walking speeds remain.

The iris authentication procedure mainly consists of 1) image acquisition, 2) iris segmentation, 3) feature extraction, and 4) pattern matching [11]. 3) and 4) require a processing time of about 3 ms [12], but 2) requires that of about 150 ms [13]. Therefore, it is impractical to apply 2) iris segmentation to all images taken at a walk-through gate. To reduce processing time, it is possible to perform high-speed image screening based on the degree of focus in 1) image acquisition. For example, a method for calculating in-focus scores based on convolution by a two-dimensional high-pass filter has been proposed [14].

B. High-speed Focus Control

A liquid lens is an optical element that changes the optical power by utilizing the interface of a fast-deforming liquid, and can operate faster than focus control by changing the relative position of heavy solid lenses [3]. Although it is sometimes referred to as a tunable lens [4], [9] or an electrically tunable lens [15], the term 'liquid lens' is used throughout this paper. There are several methods of operating principles, such as electrowetting, but this paper will focus specifically on polymer-based liquid lenses.

To effectively utilize the fast response of the liquid lenses, it is necessary to measure and evaluate the fast optical power changes with sufficient spatio-temporal resolution. The fast optical power change can be measured by using a laser beam and a photodiode [15]. The laser beam is injected into the liquid lens, the laser spot size changes due to the optical power change, and the photodiode that receives the light measures the change in current. In fact, [15] measured step responses of the polymer-based liquid lenses (10 and 16 mm apertures) from 10 to 36 kHz. The fast optical power changes can also be measured using a high-speed camera. Using a slit and prism, the change in optical power of the liquid lens is captured as a lateral displacement of the slit image based on Snell's law [4]. In fact, [4] used a 3,823-fps high-speed camera and super-resolution image processing

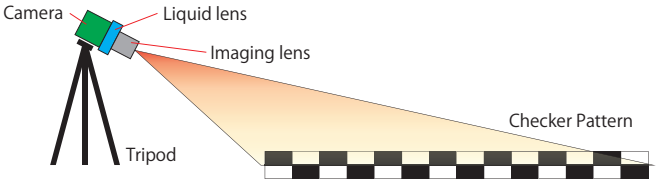

Fig. 2. Configuration of liquid lens response measurement.

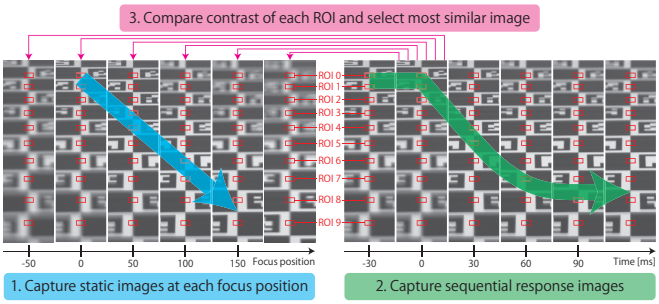

Fig. 3. Procedures of response measurement.

with intentionally tilted slits to evaluate the polymer-based liquid lens (10 and 16 mm apertures) to square waves of various frequencies (from 10 to 500 Hz). A method even with a low-speed camera [9] has also been developed based on [4]. A periodic square input (50 Hz) to the liquid lens and a camera with a frame rate slightly less than the input frequency (47.3485 fps) was used to reconstruct the response of the liquid lens [9].

When the dynamics of the liquid lens can be measured, the impulse response of the liquid lens can be estimated and the response to an arbitrary input waveform can be predicted to optimize the input to the target waveform [4], [15]. However, these methods are difficult to apply to dynamically changing target waveforms and real-time feedback control because they assume that the target waveform is known and take time to optimize. A method of optimization through closed-loop iterations that reduces deviation from the target waveform has also been developed [9]. The method does not require prior knowledge of liquid lenses or linear system control, and it is characterized by its ability to work with low-precision measurement systems because it does not require impulse response [9].

III. Image-based Response Measurement of Liquid Lens

A. System Configuration of Response Measurement

We propose a method to measure liquid lens response using a simple device configuration compared to previous studies [4], [9], [15]. The proposed system configuration is shown in Fig. 2. We attach a liquid lens for response measurement to a high-speed camera along with an imaging lens, and lay a large printed checker pattern on the floor. We tilt the high-speed camera on a tripod so that the checker pattern is in the field of view at widely different depths. As described below in Sec. III-B, we measure the temporal changes of the optical power of the liquid lens by measuring

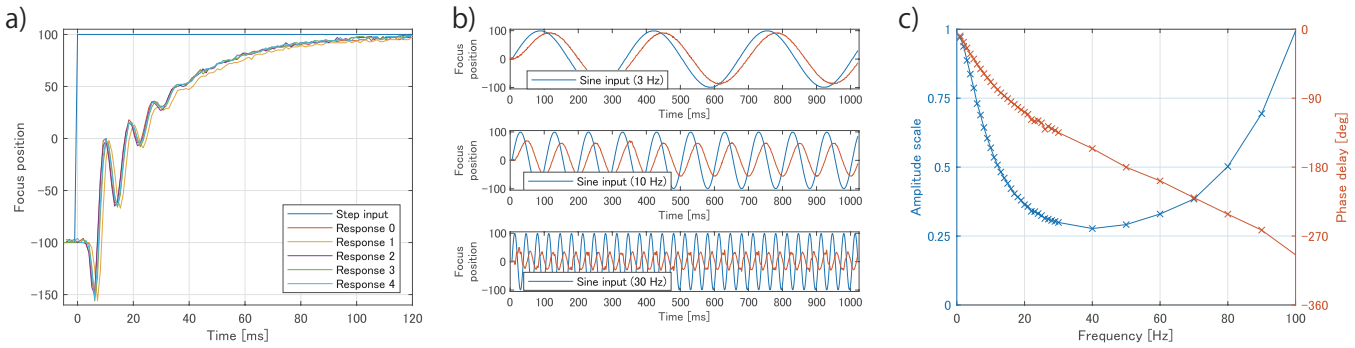

Fig. 4. Results of response measurement. a) step and b) sinusoidal responses, and c) frequency response (Bode plot).

the contrast of the edges at different depths of the checker pattern.

A feature of the proposed system configuration compared to previous studies is the simple device configuration. Although [9] is realized with a low-speed camera, a high-speed camera of about 500 fps (and even higher frame rate if reduced resolution) tends to be readily available at low cost in recent years. [4], [9] require precise alignment of the optical components including prisms, and [4], [15] require special illumination devices (e.g. a laser). Compared to these studies, the proposed method prioritizes the imaging lens attached to the response measurement over improving the spatio-temporal resolution of the response measurement. Then, for easy placement of the imaging target, which contains different depth information, we choose to capture the image from an oblique angle of the checker pattern.

B. Procedures of Response Measurement

Measurement procedures are shown in Fig. 3. First, (1) we take a sequence of static images at each focus command position within the assumed scanning range of the liquid lens. We should take care to ensure that the liquid lens response has sufficient time to converge when adjusting to each focus position. Next, (2) we capture a sequence of high-frame-rate images during the response of the liquid lens to the input to measure (e.g., step input or sinusoidal input). Finally, (3) select region of interest (ROI) at each depth position (e.g., manually), calculate the contrast values within these ROIs, and associate the focus command position with which each ROI contrast value is closest to the response image sequence. These three steps enable graphing of the temporal response of the liquid lens to an arbitrary control input.

Brenner gradient [16] is used for the contrast value, which is expressed by the following equation at k-th ROI.

$$B_k = \sum_i \sum_j \left(I_k\left(i,j\right) - I_k\left(i+m,j\right) \right)^2 , \qquad (1)$$

where $m = 2$ and $I_k\left(i,j\right)$ denotes an image pixel value inside the k-th ROI. For each contrast value $B_{f,k}$ at the focus command position f, the focus command position f_{opt} that minimizes the error is determined as follows,

$$f_{opt} = \arg\min_f \sum_k \left(B_k - B_{f,k} \right)^2 . \qquad (2)$$

C. Results of Response Measurement

We have experimentally evaluated an actual liquid lens using the proposed liquid lens response measurement method. The measured liquid lens was an Optotune EL-16-40-TC-VIS-20D-1-C (aperture, 16 mm; focal power range, ± 10 dpt). A FLIR BFS-U3-04S2M-CS (720 $\times$ 200 px, 977.927 fps) was used as a high-speed camera. The imaging lens was a motorized zoom lens, Computar VL6Z1626UC-MPYIR (focal length, from 16 to 96 mm). The liquid lens was controlled using a standard Optotune Lens Driver 4i with a 12-bit control value range of $\pm$ 4096 ($=\pm$ 293 mA). A control value of $\pm$ 100 equals $\pm$ 7.15 mA. A laptop computer Panasonic Let's note CF-SV (Windows 10) was used for real-time control. We used a checker pattern (5$\times$13 squares, 170 mm per square) with ArUco markers [17]. Note that we also used flicker-free lighting to ensure stable brightness.

Response measurement results are shown in Fig. 4. Fig. 4a) shows the response to five step inputs (control value from -100 to $+100$). Fig. 4b) shows the response to sinusoidal inputs of various frequencies (from 1 to 30 Hz in 1 Hz increments and from 40 to 100 Hz in 10 Hz increments). Fig. 4c) is a Bode plot (not in decibels or logarithms) of magnitude (amplitude scale) and phase delay based on the sinusoidal responses of Fig. 4b).

For Fig. 4a), four responses were obtained that were quite similar; only one response had a time deviation of approximately 1 ms (about 1 frame), but this was considered to be a simple synchronization delay of the command to the lens driver. This step response had the initial undershoot, which is a feature seen in a hard-to-control plant with unstable zeros [18]. Other researches have shown step responses of the same features [4], [9], [15]. Such oscillatory responses are difficult to handle in depth position estimation by focus scanning.

The nominal values of the liquid lenses are 7 ms for response time and 40 ms for settling time. The results in Fig. 4a) were slower than these nominal values, and possible reasons are differences in measurement conditions and operating environment, although the reason is unclear. In fact, a liquid lens of the same aperture (narrower optical power range, -2 to $+3$ dpt; shorter response time, 5 ms; settling time, 25 ms) also did not converge to a square input within 50 ms ([4] Fig. 4(f)).

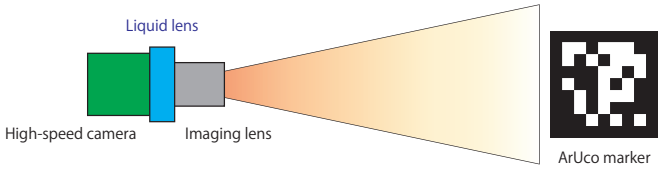

Fig. 5. System configuration of scanning calibration.

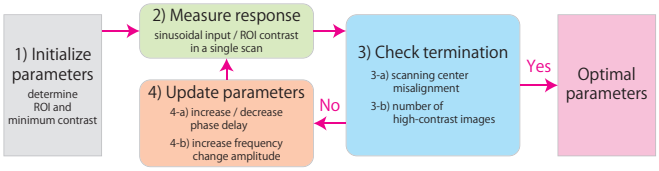

Fig. 6. Iterative procedures of scanning calibration.

Regarding the frequency response, the resonance peak is 200 Hz, and the manufacturer recommends the use of a low-pass filter for frequencies above 100 Hz. In Fig. 4c) we could actually confirm a decrease in gain at tens of Hz and an increase in gain around 100 Hz. In the calibration of scanning focus tracking described in Sec. IV, we should pay attention to these frequency characteristics of the liquid lenses.

IV. Calibration of Scanning Focus Tracking

A. Strategy of Scanning Focus Tracking

Based on the dynamic properties of the liquid lens in Sec. III, we consider a strategy for scanning focus tracking to the dynamic iris. Low latency in measurement control is necessary for tracking irregular motion targets such as up-and-down movements caused by walking, and millisecond-order sensing (e.g., 1,000 fps) such as fast pan-tilt control [2] is effective. Therefore, we select high-frame-rate imaging for the low latency and perform scanning focus control. To avoid irregularly oscillatory focus scanning as a countermeasure against eye blinking occlusion, we choose scanning with sinusoidal waves instead of square waves [4], [9].

Near the most in-focus position, the Brenner gradient in Eq. 1 can be approximated by a Lorenz function [3], [19],

$$B(z) \simeq \frac{\alpha}{\beta + (z - z_0)^2}, \tag{3}$$

where z is the focus depth position, z_0 is the target depth position, and α and β are environment-dependent parameters such as target texture. Therefore, the Brenner gradient maximum position z_0, approximated by Eq. (3) for a single scan data, is the target depth position to track.

The sinusoidal focus scanning requires feedback control every half cycle (single scan) to keep the scanning center aligned with the moving iris. Although a high sinusoidal frequency is desirable to increase the feedback rate to the dynamic iris and to increase the chances of acquiring blink avoidance images, we should be careful about the phase delay (i.e., phase inconsistency) and amplitude (i.e., depth tracking range) reduction at high frequencies (see Fig. 4c), as well as target recognition failure due to focus direction blurring. Therefore, next sections describe an iterative calibration procedure for sinusoidal frequency, amplitude, and phase delay that balances trackability for dynamic targets and recognition ability for fine texture in scanning focus tracking.

B. System Configuration of Scanning Calibration

A system configuration of scanning calibration is shown in Fig. 5. The imaging system is the same as in Sec. III, which measures the response of the liquid lens, and consists of a high-speed camera (500 fps or more) for tracking, a liquid lens for fast focus scanning, and an imaging lens. Thanks to the same device configuration, it does not require large scale conversions in response time or scanning depth range. An imaging and recognition target for the scanning calibration is an ArUco marker [17] as a substitute for the iris at a distance to be authenticated.

C. Iterative Procedures of Scanning Calibration

The sinusoidal focus scanning is formulated as follows;

$$f_l = f_c + a_l \sin\left(2\pi k_l t + \phi_l\right), \tag{4}$$

where a sinusoidal input f_l, a scanning center f_c, amplitude a_l, a frequency k_l, phase delay ϕ_l, and control time t. Because these parameters are interdependent, it is not practical to measure the control response at all parameter changes in the real-time feedback hardware of scanning focus tracking. Therefore, we should find the optimal solution dynamically updating the parameters in the real-time feedback system. The optimal parameters also need to be stable (non-divergent control) against temporal fluctuations in the feedback control loop. To easily accommodate a variety of capturing distances, lens resolutions, and control rates, we choose an iterative quasi-optimal [9] rather than analytical solution [4], [15].

The iteration procedures are shown in Fig. 6. 1) Initialize each parameter $\{\phi_l, f_c, k_l, a_l\}$, perform a low frequency scan, determin ROI around the texture (ArUco), and calculate the texture-recognizable minimum Brenner gradient B_{min}. 2) Measure the Brenner contrasts of an image sequence and input signals to the liquid lens in one scan. 3) Check termination, and if not yet converged, update the parameters in 4). 3-a) Check the misalignment of the scanning center f_c in the back and forth scans, and 4-a) increases or decreases the phase delay ϕ_l if the absolute misalignment is greater than a threshold f_{cd}. 3-b) Check the number of images above B_{min}, and 4-b) increase the frequency k_l and change amplitude a_l if the number is above a threshold N_r. When 3) reaches termination (especially 3-b), we obtain the iterative optimal parameters.

Regarding 3-a) and 4-a), since there is no mechanism for instantaneous measurement of the focal power of the liquid lens, we need to use values that take into account the latency due to the phase delay ϕ_l for response values. If the phase delay value when referring to the sinusoidal input is incorrect, different center positions f_{cf}, f_{cb} will be estimated for forward and backward scans. The phase delay is increased or decreased (0.2 ms steps) when the center position deviation $|f_{cf} - f_{cb}|$ is above the threshold

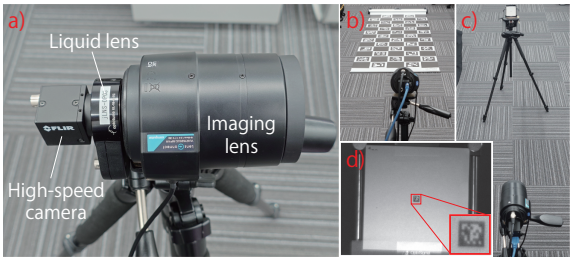

Fig. 7. Experimental system; a) imaging devices, b) setup for the response measurement in Sec. III-C, c) setup for the scanning calibration, and d) a sample captured image in the setup c).

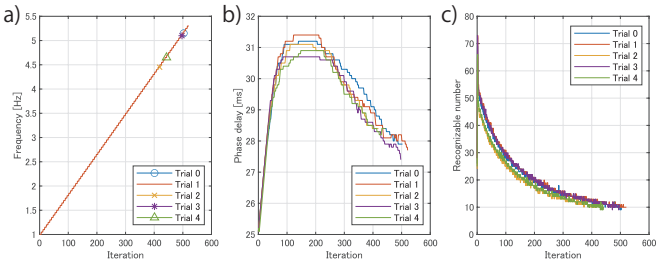

Fig. 8. Convergence results of iterative calibration; a) frequency, b) phase delay, and c) number of texture-recognizable images. One iteration refers to a half sinusoidal wave period.

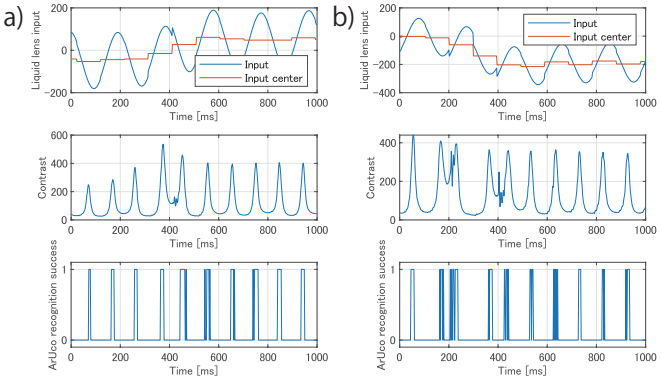

Fig. 9. Scanning focus tracking results; a) target manual movement, b) motorized zooming for a static target.

f_{cd}. When this iteration converges, the phase delay ϕ_l and scanning center f_c at the current frequency k_l are obtained.

Regarding 3-b) and 4-b), we note the amplitude attenuation in Fig. 4c). The input amplitude is increased by dividing the target amplitude a_{lt} by its attenuation coefficient (which can be obtained with a 5th order polynomial approximation in Fig. 4c), so that the same depth scanning range is maintained even if the frequency k_l is changed. The design should be such that the distance exceeds the sinusoidal half period for a human walking speed of 1.4 m/s (e.g., 140 mm at 5 Hz).

In 3-b), we need to confirm that N_r images (e.g., 10 images) or more can be recognized in a single scan. In this case, instead of the time-consuming iris recognition (150 ms for segmentation [13], 3 ms for feature extraction and pattern matching [12]) and ArUco marker recognition (more than 10 ms [17]), which inhibit real-time feedback, the Brenner contrast values are used, which can be computed much faster than 2 ms. Note that the minimum texture-recognizable contrast B_{min} front and rear the target does not coincide because the blurring changes due to differences in the point spread function (dependent on lens aberration). In this paper, the higher minimum contrast value is used as a strict condition. Note that such a strategy is similar to data cleansing for real-time object recognition with high-speed camera imaging [20].

V. EXPERIMENTAL EVALUATION

A. Experimental System

The experimental system is shown in Fig. 7. Basically the same device as in Sec. III-C, with minor changes to frame rate and other settings. The liquid lens was the Optotune EL-16-40-TC-VIS-20D-1-C (aperture, 16 mm; focal power range, $\pm$10 dpt), controlled by the Optotune Lens Driver 4i (control value range, $\pm 4096 = \pm 293$ mA). The high-speed camera was the FLIR BFS-U3-04S2M-CS (720 $\times$ 540 px, 500 fps). The imaging lens was the Computar VL6Z1626UC-MPYIR (focal length (zoom value) range, 4,111 (wide) - 17,911 (tele) = 16 - 96 mm; focus value range, 5,159 (near) - 2,739 (far)). We used a slider (Manfrotto Magic Carpet Carbon Slider, 60 cm length) to move a marker back and forth smoothly. For flicker-free observation of the marker, we used Nissin Electronic WDR-FA70 lighting (white color). The control computer was the Panasonic Let's note CF-SV.

The ArUco marker printed in 4 mm square (7 $\times$ 7 bit, 0.44 mm per spuare) was used at a distance of about 2 m from the camera. The initial zoom and focus values of the imaging lens were set to 17,000 and 3,880, respectively. The ArUco markers were observed at approximately 30 px square (3.33 px per square). With these imaging lens settings, a liquid lens control value of $\pm$100 corresponded to a depth range of approximately 400 mm at 2 m away. The depth range is possible at 1.75 Hz or higher for a 1.4 m/s walking speed, then we decided the target amplitude $a_{lt} = 100$ in this experiment. The texture-recognizable number $N_r$was set to 10. For the termination check in 3-b), the average of 5 iterations was used for stability.

B. Calibration of Scanning Focus Tracking

The iteration results of the 5 trials of calibration are shown in Fig. 8. After each half-period iteration, the frequencies converged to 4.97 Hz (average of 10 trials, standard deviation 0.30 Hz), which is well above the 1.75 Hz at the assumed 1.4 m/s walking speed. The phase delay first moved around 31 ms and then converged to around 27.7 ms (average of 10 trials, standard deviation 0.46 ms) as the frequency increased. The number of recognizable images gradually declined as the frequency increased, ending at the target of 10 images. We have confirmed that the parameters to calibrate converge to almost the same value, although there is a little variation due to the initialization process, such as variation in the texture-recognizable minimum contrast value.

Note that there is a slight difference between the response

measurement results (about 21.7 ms at 4.97 Hz, Sec. III) and the calibration results (27.7 ms, Sec. V-A) regarding the phase delay. Differences in control rates, non-consideration of temperature compensation inside liquid lenses, and difference in liquid lens orientation relative to gravity (noticeable for large apertures) are possible candidates for the cause.

C. Scanning Focus Tracking

The results of scanning focus tracking (with calibrated parameters; frequency, 5.15 Hz; phase delay, 27.9 ms) to target manual movement and motorized zoom adjustment (widening for advancing) are shown in Fig. 9. The manual movement was about 1 m/s forward from the liquid lens control value of 100 (about 0.2 m depth) displacement in 0.2 s. The sinusoidal scanning center was dynamically updated for such movement, and images were taken for each scan that ArUco could recognize (offline analysis). In the zoom adjustment (designed for maintaining adequate resolution and sufficient depth of field), there was a moment of unrecognizable time, but a recognizable scan returned before zoom convergence. The initial unrecognizable time may have been caused by rapid acceleration due to initial overshooting in the motorized zoom mechanism. The fact that ArUco recognizable scans continued after the wide-angle change (resolution reduction) to a stationary target suggests that the scan parameters were appropriately calibrated. Note that the instability of ArUco recognition at high contrast may be due to the optical characteristics of the lens. These results confirm the adequate parameter calibration of sinusoidal scanning with both target motion and texture recognition, although there is a target speed upper limit.

VI. DISCUSSION AND CONCLUSION

In this paper, we propose an image-based measurement method for liquid lens response in a situation with imaging lens and a calibration method for sinusoidal scanning focus tracking in a millisecond order real-time feedback situation for adaptive in-focus imaging utilizing the liquid lens for dynamic iris authentication. In the response measurement method, oscillatory step response and frequency response up to 100 Hz were validated using a tilted large checker pattern. The calibration of sinusoidal focus tracking allowed iterative solution of sinusoidal parameters that could correspond to human walking speed (1.4 m/s) and eye blinking occlusion (200 ms [5]), with contrast indices that could be calculated fast enough for a measurement control rate of 500 fps.

The converged frequency (about 5 Hz) depends on the texture-recognizable image number; fewer number allows a higher frequency, but are prone to more unstable feedback control. In this paper, two scans at 5 Hz that corresponds to the eye blinking occlusion time (200 ms) is interpreted as a sufficient measurement frequency.

It should be noted that [3] achieved similar scanning focus tracking based on three different depth measurement points using a high-speed liquid lens (3 mm aperture, 2 ms response) at a higher frequency than our paper results, every 15 ms (i.e., 66.7 Hz). However, this result [3] was achieved with a small aperture liquid lens, which is not appropriate for micro-texture authentication, such as iris, because its small aperture reduces optical resolution. This paper assumes a large aperture lens for high resolution for iris authentication and explores as fast response as possible with the large aperture liquid lens with slower response than [3].

In future, the same calibration and tracking will be evaluated not only for AR markers but also the iris of both printed [7] and human [1]. In combination with a high-speed pan-tilt controller using galvanometer mirrors [1], we will also realize tracking for iris that move not only in depth but also in three dimensions, and achieve dynamic iris authentication in practical situations such as walk-through gates.

REFERENCES

[1] T. Sueishi et al. Dynamic iris authentication by high-speed gaze and focus control. In 2021 IEEE/SICE International Symposium on System Integration (SII), pp. 813–814, 2021.

[2] K. Okumura et al. 1 ms auto pan-tilt–video shooting technology for objects in motion based on saccade mirror with background subtraction. Advanced Robotics, 29(7):457–468, 2015.

[3] H. Oku et al. High-speed liquid lens for computer vision. In 2010 IEEE International Conference on Robotics and Automation (ICRA), pp. 2643–2648, 2010.

[4] C. Dorronsoro et al. Tunable lenses: dynamic characterization and fine-tuned control for high-speed applications. Optics express, 27(3):2085–2100, 2019.

[5] P. P. Caffier et al. Experimental evaluation of eye-blink parameters as a drowsiness measure. European journal of applied physiology, 89:319–325, 2003.

[6] J. Li et al. Adaptive milliseconds tracking and zooming optics based on a high-speed gaze controller and liquid lenses. Optics Express, 32(2):2257–2270, 2024.

[7] Adam Czajka. Database of iris printouts and its application: Development of liveness detection method for iris recognition. In 2013 18th International Conference on Methods and Models in Automation and Robotics (MMAR), pp. 28–33, 2013.

[8] ISO/IEC 2nd CD 29794-6:201x, Information technology – Biometric sample quality – Part 6: Iris image, 2011.

[9] A. G. L. Haro et al. Closed-loop experimental optimization of tunable lenses. Applied Optics, 61(27):8091–8099, 2022.

[10] K. Nguyen et al. Long range iris recognition: A survey. Pattern Recognition, 72:123–143, 2017.

[11] YH. Li et al. Iris Recognition, Overview, Encyclopedia of Biometrics, pp. 810-819, 2009.

[12] J. Wei et al. Towards more discriminative and robust iris recognition by learning uncertain factors. IEEE Transactions on Information Forensics and Security, 17:865–879, 2022.

[13] T. Toizumi et al. Segmentation-free direct iris localization networks. In Proceedings of the IEEE/CVF Winter Conference on Applications of Computer Vision (WACV), pp. 991–1000, 2023.

[14] J. Daugman. How iris recognition works. In The essential guide to image processing, pp. 715–739, 2009.

[15] D. Iwai et al. Speeded-up focus control of electrically tunable lens by sparse optimization. Scientific reports, 9(1):12365, 2019.

[16] J. F. Brenner et al. An automated microscope for cytologic research a preliminary evaluation. Journal of Histochemistry and Cytochemistry, 24(1):100–111, 1976.

[17] S. Garrido-Jurado et al. Automatic generation and detection of highly reliable fiducial markers under occlusion. Pattern Recognition, 47(6):2280–2292, 2014.

[18] W. Ohnishi et al. Preactuated multirate feedforward control for independent stable inversion of unstable intrinsic and discretization zeros. IEEE/ASME Transactions on Mechatronics, 24(2):863–871, 2019.

[19] S. Yazdanfar et al. Simple and robust image-based autofocusing for digital microscopy. Optics express, 16(12):8670–8677, 2008.

[20] S. Namiki, et al. Online object recognition using cnn-based algorithm on high-speed camera imaging: Framework for fast and robust high-speed camera object recognition based on population data cleansing and data ensemble. In 2020 25th International Conference on Pattern Recognition (ICPR), pp. 2025–2032, 2021.